Core-Shell Double Gyroid Structure Formed by Linear ABC Terpolymer Thin Films

Ségolène Antoine, Karim Aissou, Muhammad Mumtaz, Siham Telitel, Gilles Pecastaings, Anne-Laure Wirotius, Cyril Brochon, Eric Cloutet, Guillaume Fleury, Georges Hadziioannou

Core-Shell Double Gyroid Structure Formed by Linear ABC Terpolymer Thin Films

Ségolène Antoine,[1] Karim Aissou,[1*] Muhammad Mumtaz,[1] Siham Telitel,[1] Gilles Pécastaings,[1] Anne-Laure Wirotius,[1] Cyril Brochon,[1] Eric Cloutet,[1] Guillaume Fleury,[1] and Georges Hadziioannou[1]

[1]Laboratoire de Chimie des Polymères Organiques (LCPO), CNRS - ENSCPB - Université de Bordeaux, 16 Avenue Pey-Berland, F-33607 Pessac Cedex, France

E-mail: karim.aissou@enscbp.fr

ABSTRACT: The synthesis and the self-assembly in thin film configuration of linear ABC triblock terpolymer chains consisting of polystyrene (PS), poly(2-vinylpyridine) (P2VP) and polyisoprene (PI) are described. For that purpose, a hydroxyl-terminated PS-*b*-P2VP (45 kg.mol^{-1}) building block and a carboxyl-terminated PI (9 kg.mol^{-1}) were first separately prepared by anionic polymerization, and then were coupled *via* a Steglich esterification reaction. This quantitative and metal free catalyst synthesis route revealed to be very interesting since functionalization and purification steps are straightforward and well-defined terpolymers are produced. A solvent vapor annealing (SVA) process was used to promote the self-assembly of frustrated PS-*b*-P2VP-*b*-PI chains into a thin film core-shell double gyroid (Q^{230}, space group: $Ia\bar{3}d$) structure. As terraces are formed within PS-*b*-P2VP-*b*-PI thin films during the SVA process under a $CHCl_3$ vapor, different plane orientations of the Q^{230} structure ((211), (110), (111) and (100)) were observed at the polymer-air interface depending on the film thickness.

KEYWORDS: Core-shell double gyroid structure, thin film, self-assembly, anionic polymerization, Steglich esterification.

The self-assembly of AB-type block copolymer (BCP) thin films into well-ordered nanoscale morphologies[1–3] (including spheres, cylinders, lamellae and complex networks such as the Q^{230} and O^{70} structures) provides an elegant route to create low-cost and large scale patterned surfaces with feature dimensions challenging to achieve with traditional lithography. While nanotemplates derived from the self-assembly of AB-type BCP thin films enable to achieve well-ordered features (*i.e*. dots, holes and pillars) within a common *p*6*mm* symmetry pattern due to packing frustration, a broader structural diversity has been demonstrated from linear ABC triblock terpolymer thin films, including core-shell versions of cylinders (*p*6*mm*),[4–9] alternating cylinders with a tetragonal packing (*p*2*mm*),[10,11] and two complex networks with patterns having *p*3*m*1 or *p*2 symmetries.[12] These additional pattern symmetries formed by microphase-separated ABC-type terpolymer thin films can be used to create surfaces with improved or new functionalities. For instance, three-dimensional nanostructures with "two-colored" continuous pathways sharing or not a domain interface (*i.e*. the pathways are in contact or separated) can be formed.[13–18] Such 3D unique textures open up new opportunities for electronic and ionic transports enabling the fabrication of devices with a more efficient active area.

Sequential living polymerization is an excellent methodology to achieve narrowly distributed ABC-terpolymer chains with a tunable molecular weight.[13,19–25] However, a significant limitation can be encountered in the sequential polymerization of the ABC-terpolymer if the reactivities of the A, B and C monomers do not decrease as: A > B > C.[26,27] To overcome this limitation, the different blocks can also be synthesized independently if the reactivity of the monomer B is lower than that of the C one. For instance, end-functionalized AB-type BCP chains can be firstly synthesized, then different methodologies can be used to attach them to a functionalized C homopolymer. One of the most common methods to attach the different blocks deals with "click

chemistry" reactions such as the azide-alkyne Huisgen and Diels Alder cycloadditions.[28–30] Even though a high yield can be achieved from click reactions, cycloadditions are generally catalyzed with metallic salt which could be a drawback for some technological applications. Moreover, the end-functionalization of the different polymeric chains can be challenging to achieve.

In our approach, the AB-type BCP and the C homopolymer were linked together *via* a Steglich esterification reaction which is a very convenient reaction since (*i*) the synthesis is metal free, (*ii*) the functionalization steps are straightforward and quantitative, and (*iii*) the yield of the coupling is close to unity. Indeed, living polymer chains can be easily end-capped with a hydroxyl or carboxyl function by adding a termination agent in the reactional media. For instance, Quirk[31,32] and coworkers demonstrated that it is possible to carboxylate a living chain using carbon dioxide. Another well-known end-functionalization methodology is the hydroxylation of lithium-based initiated living polymeric chains with ethylene oxide.[23]

In this work, a frustrated PS-*b*-P2VP-*b*-PI triblock terpolymer was synthesized by combining the anionic polymerization, to prepare well-defined hydroxyl-terminated PS-*b*-P2VP and carboxyl-terminated PI chains, with a coupling Steglich[33] esterification step to attach the end-functionalized diblock and homopolymer chains. The anionic polymerization of the PS-*b*-P2VP BCP was terminated with ethylene oxide to introduce a hydroxyl function at the end of the BCP chains while the homopolymer was end-capped with carbon dioxide to generate the carboxyl-terminated PI (PI-COOH). Thin film self-assembly of the PS-*b*-P2VP-*b*-PI chains promoted by a solvent annealing treatment leads to a core-shell double gyroid (DG) structure (Q^{230}). Interestingly, we demonstrated that the plane orientation of the Q^{230} structure strongly depends on the film thickness since the (211), (111) and (100) planes oriented parallel to the air surface are successively observed by decreasing the PS-*b*-P2VP-*b*-PI film thickness while the (110) plane orientation is stabilized on the step of terraces.

EXPERIMENTAL SECTION

Materials. *sec*-butyllithium (*sec*-BuLi, ~1.2 M in cyclohexane), *n*-butyllithium (*n*-BuLi, 1.6 M in hexane), dibutyl magnesium, (1 M in heptane), calcium hydride (CaH_2), sodium metal (cubes in kerosene oil) were purchased from Sigma Aldrich and used as received. Anhydrous lithium chloride was purchased from Fisher Scientific and used as received. Isoprene (I) and styrene (S) from Sigma-Aldrich were first distilled over CaH_2, then I and S were stirred with *n*-BuLi and dibutyl magnesium, respectively. 2-vinylpyridine (2VP, Sigma Aldrich) was distilled twice over CaH_2. Ethylene oxide was purified over sodium and condensed into the flask prior to use. Tetrahydrofuran (THF, Sigma-Aldrich), dried over a Braun MB-SPS-800 solvent purification system, was additionally distilled over sodium benzophenone ketyl prior to use.

Hydroxyl-terminated diblock copolymer synthesis. PS-*b*-P2VP-OH chains were synthesized using a sequential living anionic polymerization under an Ar environment. Tetrahydrofuran (THF, 40 mL), introduced into a 250 mL flame-dried round flask equipped with a magnetic stirring bar, was first cooled down to -78°C, then *sec*-butyllithium (*sec*-BuLi, 0.085 mL, ~1.2 M) was charged followed by the addition of styrene (S, 2 mL). The orange reaction mixture was stirred for 1 hour, then an aliquot of the PS block was taken before the addition of 2-vinylpyridine (2VP, 1.7 mL), and quenched with degassed methanol. PS aliquot was analyzed by size exclusion chromatography (SEC) with universal calibration to determine its molecular weight, M_n, and its dispersity, $Đ$. 2-vinylpyridine (2VP, 1.7 mL) was subsequently added to the reaction mixture and allowed to polymerize during 40 minutes, then ethylene oxide was added in the mixture, giving a colorless solution. The mixture kept stirred during 10 minutes was terminated by the addition of degassed methanol. The mixture was concentrated under reduced pressure, precipitated in cyclohexane and dried in oven at 35°C.

The end-functionalized PS-*b*-P2VP chains were characterized by proton nuclear magnetic resonance spectroscopy (^{1}H NMR, (δ (ppm), 400 MHz, CD_2Cl_2)), diffusion ordered spectroscopy (2D DOSY NMR, (δ (ppm), 400 MHz, THF-d8)), size exclusion chromatography (SEC, THF) with universal calibration, and Fourier transform infrared (FTIR) spectroscopy.

Carboxyl-terminated polyisoprene synthesis. PI-COOH was synthesized *via* an anionic polymerization in THF under an Ar atmosphere in order to avoid the dimerization which can occurs with specific solvents.[34] THF (40 mL) introduced in a 250 mL flame-dried round flask equipped with a magnetic stirrer, was cooled down to -20°C. *Sec*-BuLi (0.08mL, ~1.2M) was charged followed by the addition of isoprene (2 mL). The slightly yellow reaction mixture was stirred for 6 hours, then carbon dioxide was introduced in the flask to end-cap the PI chains. After 10 minutes, the living polymerization was terminated by adding dried methanol. The mixture was concentrated by evaporation, precipitated in methanol and dried in oven at 35°C. Carboxylic acid chain-ends were titrated with KOH (0.01 M) in presence of the phenolphthalein indicator. PI-COOH was characterized by ^{1}H NMR (δ (ppm), 400 MHz, $CDCl_3$), 2D DOSY NMR (δ (ppm), 400 MHz, THF), SEC with universal calibration in THF, and FTIR.

Esterification step between the diblock copolymer and homopolymer chains. The linear ABC terpolymer was synthesized *via* an esterification reaction between the hydroxyl-functionalized PS-*b*-P2VP and the carboxyl-terminated PI. PS-*b*-P2VP-OH (1 eq.), PI-COOH (3 eq.) and *N*,*N*-Dimethyl-4-pyridinaminium 4-methylbenzenesulfonate (DPTS, 10 eq.), introduced in a 100 mL round flask equipped with a magnetic stirring bar, were solubilized in dried dichloromethane at 40°C. After 15 minutes, *N*,*N*′-Diisopropylcarbodiimide (DIC, 10 eq.) was introduced in the flask, then the mixture was allowed to react during 3 days. Once the reaction was completed, DPTS was recovered by precipitation in THF then separated from the mixture. Excess

of PI-COOH was separated from the PS-*b*-P2VP-*b*-PI terpolymer by precipitation in heptane. The linear PS-*b*-P2VP-*b*-PI terpolymer was characterized by ^{1}H NMR (δ (ppm), 400 MHz, CD_2Cl_2), 2D DOSY NMR (δ (ppm), 400 MHz, THF-d8), SEC with universal calibration in THF, and FTIR.

Results and Discussion

The synthetic route to the linear PS-*b*-P2VP-*b*-PI triblock terpolymer chain is presented in **Figure 1**. PS-*b*-P2VP chains were prepared by a sequential anionic polymerization of styrene and 2-vinyl pyridine monomers in THF at -78°C under an argon atmosphere using *sec*-BuLi as an initiator. The reaction was terminated by the addition of ethylene oxide (EO) to produce a hydroxyl-terminated PS-*b*-P2VP BCP. The propagation of ethylene oxide was prevented (*i.e.* only one EO unit was added) since Li was used as counter anion.[35] The PI homopolymer was also prepared *via* an anionic polymerization in THF at -20°C under an Ar atmosphere using *sec*-BuLi as initiator. The living PI chains have a high reactive carbanion capable to react in a quantitative way with the carbon dioxide. Therefore CO_2 was added at the end of the reaction to achieve a carboxyl-terminated PI homopolymer. The linear PS-*b*-P2VP-*b*-PI triblock terpolymer was produced *via* an esterification reaction between PS-*b*-P2VP-OH and PI-COOH with DIC as coupling reagent and DPTS as catalyst. The addition of DPTS is important to increase the yield of the ester since this catalyst suppresses the formation of unwanted *N*-acylurea.

SEC with universal calibration curves and ^{1}H NMR spectra of the PI (blue), PS-*b*-P2VP (red), and PS-*b*-P2VP-*b*-PI (black) chains are presented on **Figure 2a-b**. ^{1}H NMR spectrum of the PI homopolymer shows the characteristic peaks of the 1.2 (δ = 5.5 – 6 ppm) and 3.4 (δ = 4.4 – 5 ppm) units. According to the integration peak areas relative on the NMR spectrum, the PI homopolymer contains 3.4 and 1.2 in-chain units in a 3.4:1.2 ratio close to 7:3.[36,37] The molecular weight of the end-functionalized PI homopolymer was determined to be 9 kg.mol^{-1} with a dispersity, *Đ*, of 1.2

from the SEC curve. As the quantitative functionalization of PI cannot be confirmed by ^{1}H NMR, the carboxylic acid chain-ends were titrated with KOH using phenolphthalein as colorant indicator. The titration confirmed the quantitative functionalization of the PI-COOH. During the synthesis of the PS-*b*-P2VP-OH, an aliquot was taken at the end of the styrene polymerization to determine the PS molecular weight. The SEC trace of the PS (pink) chains exhibits a narrow, monomodal peak corresponding to a molecular weight of 21 kg.mol^{-1} ($Đ$ = 1.1). At the end of the PS-*b*-P2VP-OH synthesis, the PS volume fraction was found to be 0.48 by ^{1}H NMR. This composition is in accordance with the PS-*b*-P2VP-OH SEC trace from which a molecular weight and a dispersity of 45 kg.mol^{-1} and 1.1, respectively, were determined. The SEC trace showed a shoulder in the lower molecular weight region next to the original PS-*b*-P2VP-OH peak which is due to the presence of PS homopolymer. As a quantitative end-functionalization of the PS-*b*-P2VP-OH BCP proved difficult to evidence by either ^{1}H NMR or even by FTIR, a good way to confirm the presence of the hydroxyl group was to couple the PS-*b*-P2VP-OH BCP with the PI-COOH homopolymer *via* an esterification step. A shift of the PS-*b*-P2VP-*b*-PI SEC curve towards a higher molecular weight region than that of the original PS-*b*-P2VP-OH BCP demonstrated the successful formation of the targeted linear ABC triblock terpolymer having a molecular weight and a dispersity of 54 kg.mol^{-1} and 1.1, respectively. It is noteworthy that a small shoulder can be observed on the PS-*b*-P2VP-*b*-PI SEC trace which indicates that some PS homopolymer chains still remain within the targeted PS-*b*-P2VP-*b*-PI terpolymer.

Further evidence of the coupling between the PI-COOH and PS-*b*-P2VP-OH chains was obtained by 2D-DOSY-NMR (see **Fig. 3**). From the 2D-DOSY spectra, the diffusion coefficients of PS-*b*-P2VP-OH and PI-COOH were found to be 1.7 x 10^{-10} m^{2}.s^{-1} and 7.42 x 10^{-11} m^{2}.s^{-1}, respectively (spectra not showed here). After coupling, the NMR experiment revealed that ^{1}H

resonances belonging to PS, P2VP and PI are aligned with the same horizontal line for the PS-*b*-P2VP-*b*-PI terpolymer. This indicates that all signals arise from the same macromolecule which have a higher diffusion coefficient (D = 4.48 x 10^{-10} $m^2.s^{-1}$) than that of PI-COOH and PS-*b*-P2VP-OH. It is noteworthy that not aligned signals with the horizontal line are due to solvents.

The thin film morphology formed by the frustrated PS-*b*-P2VP-*b*-PI terpolymer chains ($\chi_{PS\text{-}PI}$[38] : $\chi_{PS\text{-}P2VP}$[39] : $\chi_{P2VP\text{-}PI}$[40] ≈ 1 : 1 : 8) was also studied. For that purpose, a 2 wt. % polymer solution in toluene was spin-coated on silicon substrates and the film thickness was controlled by the spin-coating speed (1.5 krpm). The PS-*b*-P2VP-*b*-PI self-assembly was achieved by exposing samples to a continuous stream of a $CHCl_3$ vapor produced by bubbling nitrogen gas through the liquid solvent as described previously.[9,41,42] The morphology of the solvent-annealed PS-*b*-P2VP-*b*-PI thin films was frozen by quickly removing the lid of the chamber. As the $CHCl_3$ vapor used for the solvent annealing process favors the formation of a PI top surface layer, a fluorine-rich reactive ion etch (RIE) plasma was applied to remove this low surface energy layer which revealed the thin film morphology (plasma conditions: 40 W, 17 sccm CF_4 and 3 sccm O_2, 180 mTorr, and 45 s).

Importantly, the PS-*b*-P2VP-*b*-PI layers are split into terraces (*i.e*. regions with different film thicknesses) during the SVA process under a chloroform vapor. Atomic force microscopy (AFM) topographic images presented on **Figure 4a-b** show different terraces of a solvent-annealed (2h, $CHCl_3$) PS-*b*-P2VP-*b*-PI thin film treated by CF_4/O_2 RIE plasma. After preferentially removing the PI (black) domains with a fluorine-rich plasma, the characteristic (211) crystallographic plane of the Q^{230} structure oriented parallel to the air surface can be observed on the upper terraces of PS-*b*-P2VP-*b*-PI layer having a thickness of ~190 nm (see **Fig. 4a**). In contrast, a *p*6*mm* symmetry pattern with a period of ~57 nm is observed on the regions of the PS-*b*-P2VP-*b*-PI layer having a

thickness of ~90 nm (see **Fig. 4b**). This pattern oriented parallel to the air surface can be attributed to the (111) plane of the core-shell gyroid structure. Interestingly, this core-shell gyroid structure is not the equilibrium morphology in bulk since the synchrotron small angle X-ray scattering (SAXS) pattern of the PS-*b*-P2VP-*b*-PI powder exhibits a first-order peak, q^*, at 0.165 nm^{-1} and higher-order peaks located at $q/q^* = 1, 2, 3$ and 4 consistent with a lamellar phase having a period of ~38.1 nm (see **Fig. S1**). This phenomenon is mainly due to the fact that the swelling ratios of the different blocks are not the same under a chloroform vapor which varies the effective block compositions. Indeed, the chloroform is a strong selective solvent for the PI homopolymer which reaches a plateau for a thickness variation of 90%, while the PS and P2VP homopolymers reach their plateau for a 35% thickness variation as measured from a reflectometer apparatus with a UV-visible spectral range.

To gain insight about the thin morphologies developed within the (211) and (111) planes, PS-*b*-P2VP-*b*-PI thin films were also plunged in a H_2PtCl_6 solution in order to increase the durability of H_2PtCl_6-stained P2VP domains under the RIE plasma conditions and so, to improve the AFM topographic image contrast. AFM topographic views presented in **Figure 4c-d** show solvent-annealed (2h, $CHCl_3$) 190 and 90 nm thick regions of the PS-*b*-P2VP-*b*-PI layer immersed into an aqueous H_2PtCl_6 solution then subsequently treated by a CF_4/O_2 RIE plasma. A (211) plane oriented parallel to the air surface with its typical “double-wave” pattern, consisting of small- and large-amplitude oscillations, can be clearly observed from a 190 nm thick PS-*b*-P2VP-*b*-PI layer (see **Fig. 4c**). This double wave pattern has a long period of ~120 nm which gives a good indication of the unit cell dimension, a_G. In contrast, a “wagon-wheel” pattern, consisting of 6-fold H_2PtCl_6-stained P2VP (bright) domains surrounded by smaller PI (black) and PS (brown) domains, is observed on terraces having a thickness of ~90 nm (see **Fig. 4d**).

Scanning electron microscopy (SEM) images presented in **Figure 5** show additional plane orientations of the core-shell DG structure produced from solvent-annealed (2h, $CHCl_3$) PS-*b*-P2VP-*b*-PI layers plunged into an aqueous H_2PtCl_6 solution then subsequently treated by CF_4/O_2 RIE plasma. The hexagonal pattern showed in **Figure 5a** is consistent with the "doughnut pattern" observed along the (110) projection of the Q^{230} structure. Here, etched PI (black) domains, ordered into a hexagonal array with a period of ~100 nm, are surrounded by a H_2PtCl_6-stained P2VP (light) shell in a PS (gray) matrix. Importantly, this pattern is stabilized in peculiar regions of the film where the film thickness is between the upper and lower terraces occupied by the double-wave and wagon-wheel patterns, respectively. Decreasing the film thickness well-below the unit cell dimension ($t \approx 75$ nm $< a_G$) leads to the formation of a poorly-ordered structure which resembles to the characteristic "zigzagging" lamellar pattern formed along the (100) of the Q^{230} structure (see **Fig. 5b**). This pattern with a period of ~54 nm consists of zigzagging PS (gray) and H_2PtCl_6-stained P2VP (light) lamellar domains with PI (black) domains not perfectly distributed within the P2VP lamellae.

Thin films of a Q^{230} structure with characteristic crystallographic planes such as (211), (110), (111) and (100) oriented parallel to air surface are observed depending on the layer thickness. When the film thickness is well-above the unit cell dimension ($a_G \sim 120$nm), a double-wave (211) pattern maximizing the PI composition at the polymer-air interface is produced. As the $CHCl_3$ vapor preferentially attracts the low surface tension block at the film free surface, a PI top-coat layer on the Q^{230} morphology having its (211) plane oriented parallel to the air surface appears as the thermodynamic stable structure on the upper terrace regions of the PS-*b*-P2VP-*b*-PI layer having a thickness of ~ 190 nm. Such a plane orientation, recently observed from solvent-annealed DG-forming AB-type BCP thin films having a low surface energy wetting layer,[9] allows to maximize

the area fraction of the low surface energy block at polymer-air interface as demonstrated by Hashimoto and co-workers.[43] Indeed, these authors showed that the area fraction of the minor phase along several crystallographic planes is higher than the BCP chain composition, and decreases as: (210) > (110) > (111) > (100) > BCP chain.

When the film thickness is on the order of the unit cell dimension, a hexagonal doughnut pattern with a higher surface PI composition ratio than that of PS-*b*-P2VP-*b*-PI chains is observed at the polymer-air interface. Although this Q^{230} (110) pattern does not optimize the PI composition at the free surface like the double wave pattern, it exhibits a hexagonal array with a periodicity lower than a_G which probably drives by commensurability effects a such plane orientation of the core-shell DG structure at the air surface. Decreasing again the film thickness to 90 nm makes that the (111) plane oriented parallel to the air surface is stabilized. This pattern with a PI area fraction at the free-surface slightly higher than that of PS-*b*-P2VP-*b*-PI chains exhibits, however, a hexagonal array with a period two times smaller than that of the one formed on the Q^{230} (110) pattern. Finally, a zigzagging lamellar pattern having a period of ~50 nm and a surface PI composition ratio close to the one of PS-*b*-P2VP-*b*-PI chains is produced when the film thickness is about 75 nm. Such a phase behavior indicates that the different crystallographic plane orientations on terraces are driven by two phenomenons which are the commensurability of the pattern period with the film thickness and the preferential segregation of the PI block at the free-surface.

In this communication, a metal free coupling methodology, with a yield close to unity, was used to achieve a well-defined linear PS-*b*-P2VP-*b*-PI terpolymer from end-functionalized PS-*b*-P2VP-OH and PI-COOH chains. A thin film core-shell DG structure having different plane orientations depending on the film thickness was demonstrated from solvent-annealed PS-*b*-P2VP-

b-PI terpolymer chains. The DG structure with its (211) plane oriented parallel to air surface appears as the thermodynamic stable phase when a $CHCl_3$ vapor used for the SVA process since it maximizes the area fraction of the low surface energy block at the free surface. However, commensurability effects between the plane period pattern and the terrace thickness take place when the film thickness is smaller than the unit cell dimension. A balance between the commensurability effects and the preferential attraction of the low surface energy block at polymer-air interface is discussed to explain the formation of different plane orientations on the terraces of the thin Q^{230} structure.

Acknowledgements

The authors acknowledge support from Arkema and the Nouvelle Région Aquitaine. This work was performed within the framework of the Equipex ELORPrintTec ANR-10-EQPX-28-01 and the LabEx AMADEUS ANR-10-LABEX-0042-AMADEUS with the help of the French state Initiative d'Excellence IdEx ANR-10-IDEX-003-02 and the LCPO-Arkema INDUSTRIAL CHAIR "HOMERIC" ANR-13-CHIN-0002-01. S.A. is grateful to the Région Aquitaine for financial support (Ph.D. grant #2014-1R110205-00002959).

References:

[1] F. S. Bates, G. H. Fredrickson, *Annu. Rev. Phys. Chem.* **1990**, *41*, 525–557.

[2] M. W. Matsen, M. Schick, *Phys. Rev. Lett.* **1994**, *72*, 2660–2663.

[3] M. W. Matsen, *Macromolecules* **2012**, *45*, 2161–2165.

[4] S. Guo, J. Rzayev, T. S. Bailey, A. S. Zalusky, R. Olayo-Valles, M. A. Hillmyer, *Chem. Mater.* **2006**, *18*, 1719–1721.

[5] V. P. Chuang, C. A. Ross, P. Bilalis, N. Hadjichristidis, *ACS Nano* **2008**, *2*, 2007–2014.

[6] S. M. Jeon, K. Y. Jang, S. H. Lee, H. W. Park, B. H. Sohn, *Langmuir* **2008**, *24*, 11137–11140.

[7] V. P. Chuang, C. A. Ross, J. Cwyther, I. Manners, *Adv. Mater.* **2009**, *21*, 3789–3793.

[8] M. D. Rodwogin, A. Baruth, E. A. Jackson, C. Leighton, M. A. Hillmyer, *ACS Appl. Mater. Interfaces* **2012**, *4*, 3550–3557.

[9] K. Aissou, M. Mumtaz, P. Marcasuzaa, C. Brochon, E. Cloutet, G. Fleury, G. Hadziioannou, *Small* **2017**, *13*, 1603184.

[10] V. P. Chuang, J. Gwyther, R. A. Mickiewicz, I. Manners, C. A. Ross, *Nano Lett.* **2009**, *9*, 4364–4369.

[11] H. K. Choi, J. Gwyther, I. Manners, C. A. Ross, *ACS Nano* **2012**, *6*, 8342–8348.

[12] K. Aissou, M. Mumtaz, A. Alvarez-Fernandez, J. Mercat, S. Antoine, G. Pécastaings, V. Ponsinet, C. Dobrzynski, G. Fleury, G. Hadziioannou. *Macromol. Rapid Commun.* **2018** DOI: 10.1002/marc.1700754.

[13] Y. Mogi, H. Kotsuji, Y. Kaneko, K. Mori, Y. Matsushita, I. Ichiro, *Macromolecules* **1992**, *25*, 5408–5411.

[14] T. A. Shefelbine, M. E. Vigild, M. W. Matsen, D. A. Hajduk, M. A. Hillmyer, E. L. Cussler, F. S. Bates, *J. Am. Chem. Soc.* **1999**, *121*, 8457–8465.

[15] H. Hückstädt, A. Göpfert, V. Abetz, *Polymer* **2000**, *41*, 9089–9094.

[16] T. S. Bailey, C. M. Hardy, T. H. Epps, F. S. Bates, *Macromolecules* **2002**, *35*, 7007–7017.

[17] T. S. Bailey, H. D. Pham, F. S. Bates, *Macromolecules* **2001**, *34*, 6994–7008.

[18] T. H. Epps, J. Chatterjee, F. S. Bates, *Macromolecules* **2005**, *38*, 8775–8784.

[19] H. Watanabe, T. Shimura, T. Kotaka, M. Tirrell, *Macromolecules* **1993**, *26*, 6338–6345.

[20] E. Giebele, R. Stadler, *Macromol. Chem. Phys.* **1997**, *198*, 3815–3825.

[21] C. Tsitsilianis, I. Katsampas, V. Sfika, *Macromolecules* **2000**, *33*, 9054–9059.

[22] N. Ekizoglou, N. Hadjichristidis, *J. Polym. Sci. Part A Polym. Chem.* **2001**, *39*, 1198.

[23] R. Shell, J. Gohy, N. Willet, S. Varshney, J. Zhang, R. Je, *Angew. Chemie Int. Ed.* **2001**, *40*, 3214–3216.

[24] R. Bieringer, V. Abetz, A. H. E. Müller, *Eur. Phys. J. E* **2001**, *5*, 5–12.

[25] X. S. Wang, M. A. Winnik, I. Manners, *Macromolecules* **2002**, *35*, 9146–9150.

[26] R. P. Quirk, Q. Zhuo, S. H. Jang, Y. Lee, G. Lizarraga, *Symp. A Q. J. Mod. Foreign Lit.* **1998**, DOI 10.1021/bk-1998-0696.ch001.

[27] D. Baskaran, A. H. E. Müller, *Prog. Polym. Sci.* **2007**, *32*, 173–219.

[28] K. Aissou, A. Pfaff, C. Giacomelli, C. Travelet, A. H. E. Müller, R. Borsali, *Macromol. Rapid Commun.* **2011**, *32*, 912–916.

[29] R. Huisgen, *Angew. Chemie Int. Ed. English* **1963**, *2*, 633–645.

[30] G. Franc, A. K. Kakkar, *Chem. Soc. Rev.* **2010**, *39*, 1536.

[31] R. P. Quirk, J. Yin, L. J. Fetters, *Macromolecules* **1989**, *22*, 85–90.

[32] R. P. Quirk, Y. Guo, C. Wesdemiotis, M. A. Arnould, *J. Polym. Sci. Part A Polym. Chem.* **2003**, *41*, 2435–2453.

[33] H. Erothu, A. A. Sohdi, A. C. Kumar, A. J. Sutherland, C. Dagron-Lartigau, A. Allal, R. C. Hiorns, P. D. Topham, *Polym. Chem.* **2013**, *4*, 3652.

[34] R. P. Quirk, W.- C. Che, *Macromol. Chem.* **1982**, *183*, 2071.

[35] C. Tonhauser, H. Frey, *Macromol. Rapid Commun.* **2010**, *31*, 1938.

[36] S. Bywater, D. J. Worsfold, *Can. J. Chem.* **1967**, *45*, 1821–1824.

[37] S. Worsfold, D. J.; Bywater, *Can. J. Chem.* **1964**, *42*, 2884–2892.

[38] Y. Ren, T. P. Lodge, M. A. Hillmyer, *Macromolecules* **2000**, *33*, 866–876.

[39] M. R. Hammond, E. Cochran, G. H. Fredrickson, E. J. Kramer, *Macromolecules* **2005**, *38*, 6575–6585.

[40] Y. Funaki, K. Kumano, T. Nakao, H. Jinnai, H. Yoshida, K. Kimishima, K. Tsutsumi, Y. Hirokawa, T. Hashimoto, *Polymer* **1999**, *40*, 7147–7156.

[41] K. Aissou, H. K. Choi, A. Nunns, I. Manners, C. A. Ross, *Nano Lett.* **2013**, *13*, 835–839.

[42] Y. Li, H. Huang, T. He, Y. Gong, *Appl. Surf. Sci.* **2011**, *257*, 8093–8101.

[43] T. Hashimoto, Y. Nishikawa, K. Tsutsumi, *Macromolecules* **2007**, *40*, 1066–1072.

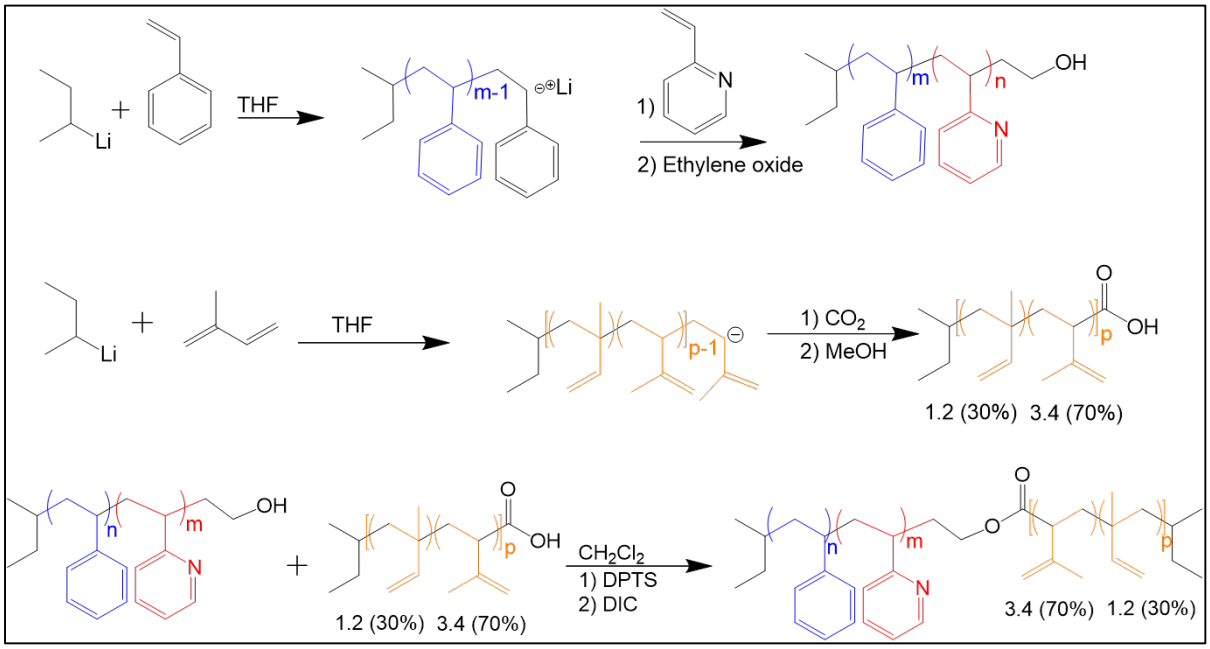

Figure 1: General route for the anionic polymerization of the PS-*b*-P2VP-OH and PI-COOH chains and their coupling *via* a Steglich esterification step.

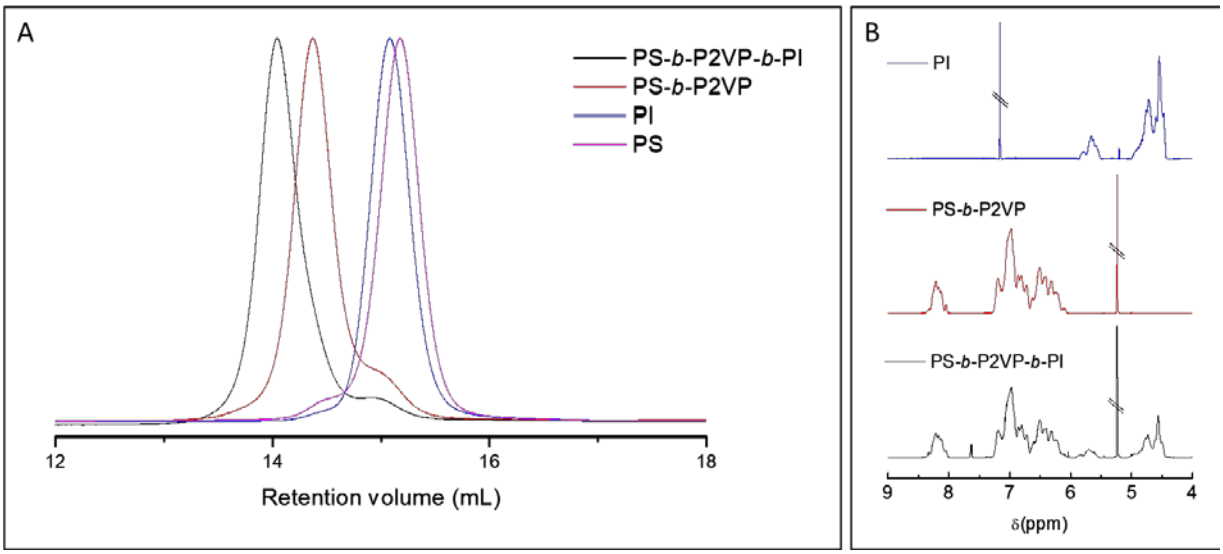

Figure 2: (a) THF-SEC with universal calibration curves (RI signal) of PI, PS-b-P2VP, PS-*b*-P2VP-*b*-PI chains. (b) ^{1}H NMR spectra of (top) PI in $CDCl_3$, (middle) PS-*b*-P2VP in CD_2Cl_2, and (bottom) PS-*b*-P2VP-*b*-PI in CD_2Cl_2

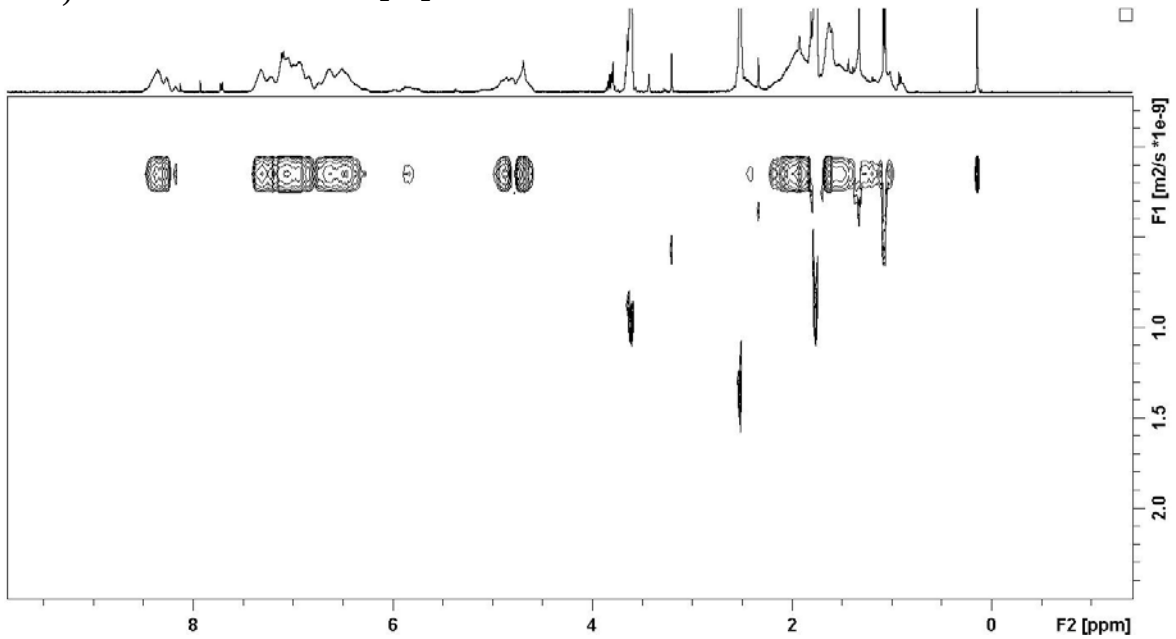

Figure 3: 2D DOSY NMR spectrum (400 MHz, THF-d8, 298K) of the PS-*b*-P2VP-*b*-PI terpolymer.

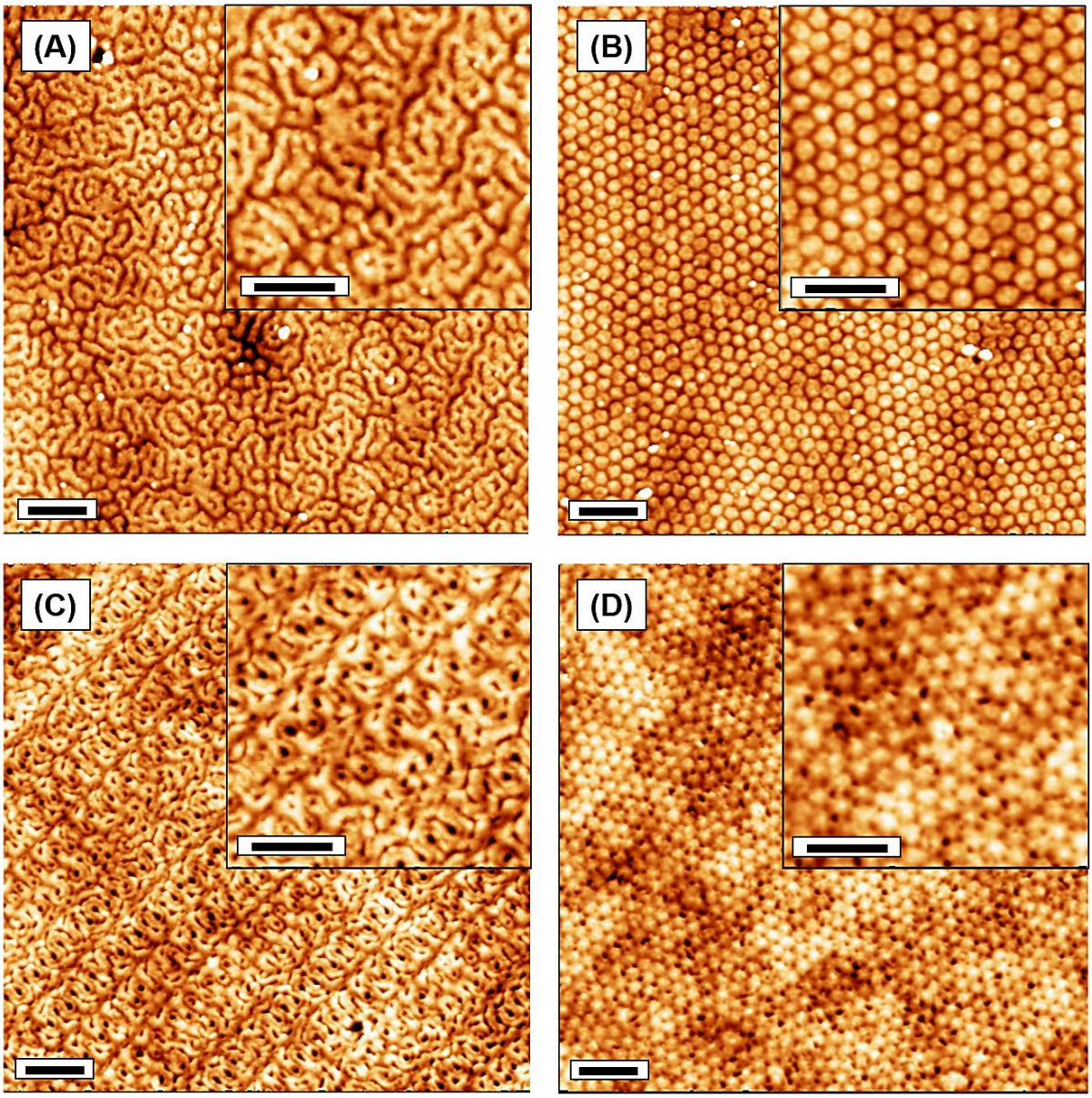

Figure 4: Low and high magnification AFM topographic views of solvent-annealed (2h, $CHCl_3$) PS-*b*-P2VP-*b*-PI layers having different film thicknesses: (a-c) 190 nm and (b-d) 90 nm. (a-b) Unstained and (c-d) H_2PtCl_6-stained PS-*b*-P2VP-*b*-PI thin films were treated by CF_4/O_2 RIE plasma. Scale bars: 200 nm.

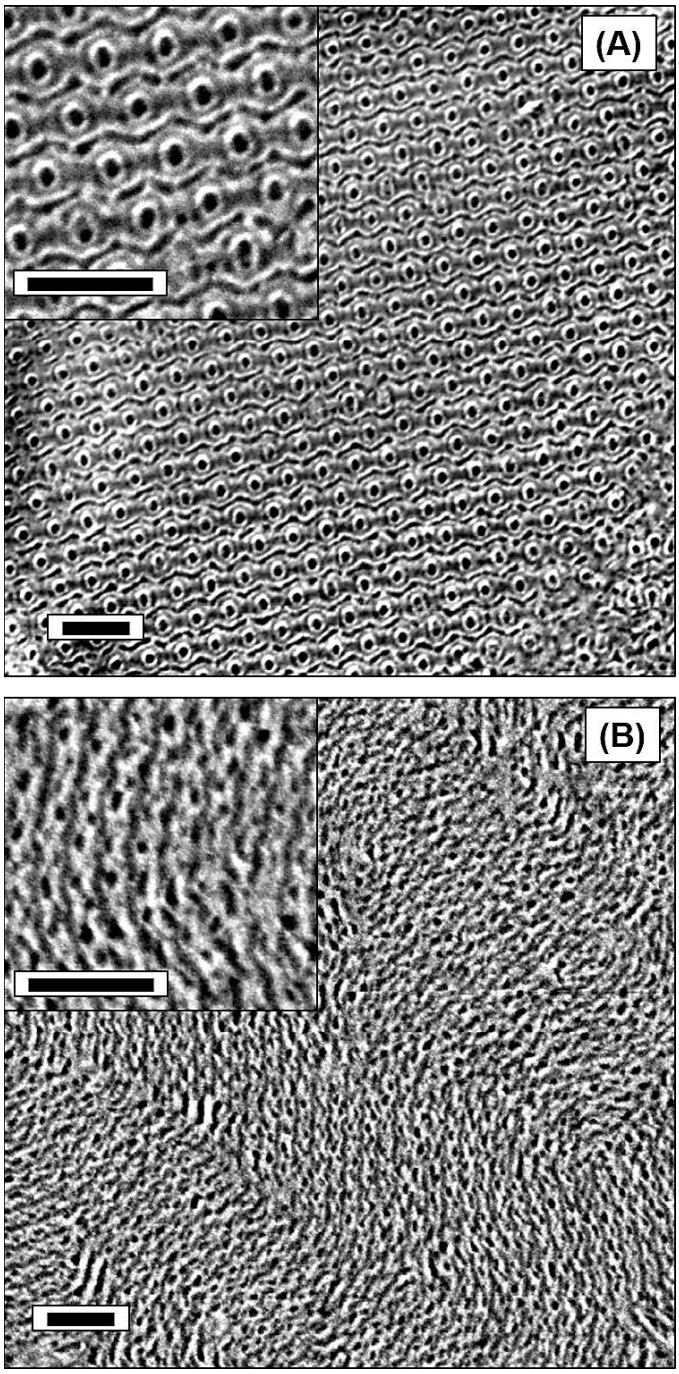

Figure 5: Low and high magnification SEM images of solvent-annealed (2h, $CHCl_3$) PS-*b*-P2VP-*b*-PI layers having different film thicknesses: (a) 140 nm and (b) 75 nm. The H_2PtCl_6-stained PS-*b*-P2VP-*b*-PI thin films were treated by CF_4/O_2 RIE plasma. Scale bars: 200 nm.

Use for table of content only